Fluid evolution in the Pedra Preta wolframite ore deposit, Paleoproterozoic Musa granite, eastern Amazon craton, Brazil

Francisco Javier Rios[a,*,1], Raimundo Netuno Villas[b,2], Kazuo Fuzikawa[a]

[a]*CDTN-CNEN-Centro de Desenvolvimento da Tecnologia Nuclear, Comissão Nacional de Energia Nuclear, Laboratório de Inclusões Fluidas e Metalogênese, Caixa Postal 941, CEP 30123-970 Belo Horizonte, MG, Brazil*
[b]*Departamento de Geologia, Centro de Geociências, Universidade Federal do Pará, Caixa Postal 1611, CEP 66075-900 Belém, PA, Brazil*

Abstract

The Pedra Preta wolframite ore deposit is hosted by a vein system that cuts rocks of the Archean Andorinhas supergroup and the cupola of the 1.88 Ga Musa granite. Several hydrothermal events have been recognized in the deposit area. The first is represented by pre-ore-stage veins that formed prior to the emplacement of the Musa granite. The second involved F-poor aqueous fluids (probably with CO_2) exsolved from the crystallizing magma, which mixed with the host rock pore fluids, which contained CH_4 and N_2, and accounted for the ore-stage veins that formed along fracture planes at 2 Kbar pressures. The third event resulted from the reopening of older sealed fractures and served as a channelway for a reducing, metamorphic, CH_4-bearing fluid. The oxidizing environment generated by that intrusion led to a substantial transformation of CH_4 into CO_2 at the site of emplacement. Late in the circulation of this fluid, wolframite crystallized at 330 °C. The fourth event was an F metasomatism (topaz and fluorite) related to H_2O and CO_2 fluids. The fifth and final hydrothermal event resulted from tectonic relaxation and formation of post-ore-stage veins by highly saline fluids (42 wt% $CaCl_2$ equivalent) at the beginning and ≈ 30 wt% NaCl equivalent toward the end at 1.0 Kbar and less than 220 °C conditions. Most evidence drawn from the fluid inclusion studies points to the metamorphic fluids as the main W mineralizing solutions, not the Musa magmatic solutions.
© 2002 Elsevier Science Ltd. All rights reserved.

Keywords: Musa granite; Wolframite; Fluid inclusions

1. Introduction

Since 1967, the Carajás Mineral Province in the southeastern Amazon craton has been the focus of important iron, manganese, bauxite, copper, gold, and nickel ore discoveries. The Pedra Preta wolframite deposit is part of this enormous mineral source, located 40 km southwest of the town of Rio Maria, southern Pará state. Presently, the Pedra Preta deposit is the main tungsten commodity of the Amazon region with ore reserves estimated at 508,000 tons (Docegeo, 1984). Together with the Seridó scheelite deposits in Rio Grande do Norte, they represent the most important known W reserves in Brazil (Willing, 1986).

Few geological studies have been performed on the Pedra Preta deposit to date. Other than work by Cordeiro and da Silva (1986), Santos (1987), and Cordeiro et al. (1988), no data have been published on the geology of the deposit, and there is no information available on the nature of the fluids responsible for the tungsten mineralization. The current research was carried out to characterize the wolframite mineralizing fluids and put some constraints on the genesis of the deposit. In addition to isotope analyses of the ore minerals, fluid inclusion (FI) microthermometry, micro-Raman spectroscopy, synchroton X-ray fluorescence, and micro-infrared studies were performed to reach those objectives.

2. Regional geological setting

The Itacaiunas shear belt (at north) and the Rio Maria granitoid–greenstone terrain (at south) form the two

* Corresponding author. Tel.: +55-31-34-99-33-54; fax: +55-31-49-93-390.

E-mail addresses: javier@urano.cdtn.br (F.J. Rios), netuno@ufpa.br (R.N. Villas).

1 www.cdtn.br/labif

2 Fax: +55-91-2111478.

Table 1
Available geochronological ages for some lithological units that form the southern part of the Carajás Mineral Province

Eras	Ga	Rio Maria granitoid–greenstone terrane		
		Complexes or supergroups	Groups or formations	Intrusive rocks
Proterozoic	1.9			Anorogenic granites (Musa, Jamon, Bannach, Gradaús, Seringa, etc.)
Archean	2.5			
	2.6		Rio Fresco Group	
	2.8			Mata Surrão and Xinguara granites, Mogno trondhjemite, Rio Maria granodiorite, Parazonia tonalite
			Tucumã, Sapucaia (?), Gradaús (?) Groups	
	2.9	Andorinhas and Serra do Inajá Supergroups	Lagoa Seca/Babaçu and Rio Preto/Santa Lúcia Groups	Arco Verde tonalite and Serra Azul ultramafic intrusion
	2.9	Xingu Complex		
	3.0			

tectonic blocks into which the Carajás Mineral Province has been divided (Araujo et al., 1988). The oldest units in the southern block (Table 1), where the Pedra Preta deposit is located, include the Xingu complex, the Arco Verde metatonalites (Althoff et al., 1995), and the Andorinhas supergroup (Hirata et al., 1982), which provide U–Pb ages of 2974 ± 15, 2957 ± 16, and 2904 ± 22 Ma, respectively (Macambira and Lancelot, 1991, 1992; Avelar et al., 1999).

The Andorinhas supergroup is a typical greenstone sequence that is stratigraphically divided into the Babaçu group (basal unit) and the Lagoa Seca group (upper unit). Main rock types of the Babaçu group include metamorphosed komatiitic and basaltic flows with intercalations of banded iron formations, schists, and metachert. The Lagoa Seca group consists of clastic and chemical metasedimentary rocks intercalated with metavolcanic rocks that vary from ultramafic to felsic. U–Pb ages of zircons from the Lagoa Seca group volcanic rocks (2970 ± 7 Ma) have been interpreted as the crystallization age of the original magma (Pimentel and Machado, 1994). Both the Arco Verde tonalite and the Andorinhas supergroup formerly were included in the Xingu complex (regional basement), but systematic fieldwork and geochronological data have restricted the latter unit to a few exposures (gneisses and high-grade schists) around the towns of Xinguara and Tucumã. Granitoid bodies (Rio Maria granodiorite, Mogno trondhjemite, Parazonia tonalite, and Mata Surrão, Xinguara, and Guarantã granites, among others) intrude the Andorinhas supergroup rocks and yield ages from 2876 to 2858 Ma (Macambira and Lancelot, 1991, 1992; Rodrigues et al., 1992; Pimentel and Machado, 1994; Macambira and Lafon, 1994).

Overlying these rock units is a transgressive cover, the Rio Fresco group, which is composed predominantly of anchimetamorphic siliciclastic sedimentary rocks of unknown age. To the north, in Serra dos Carajás, a similar sequence (Aguas Claras Formation) is cut by mafic sills and dikes that have been dated at 2645 ± 12 Ma (Dias et al., 1996). If the sedimentary units are synchronous, a rather long break in the stratigraphic record, interrupted at the onset of the widespread granitic magmatism around 1.9 Ga, must have occurred in the Rio Maria region. This Paleoproterozoic magmatic event caused the rise of several anorogenic granitic intrusions (e.g. Musa granite dated at 1883 ± 5 Ma, Machado et al., 1991) whose emplacement and related processes mark the final consolidation of the eastern block of the Amazon craton (Dall'Agnol et al., 1994).

On the eastern border of the block, the Neoproterozoic N–S-trending Araguaia belt was formed during the Brasiliano (= Pan-African) cycle (Moura and Gaudette, 1993). The effects of this geotectonic event were recorded in the nearby Rio Maria region as the reactivation of old fracture surfaces.

3. Geology of the Pedra Preta ore deposit

In the deposit area, there are outcropping rocks of the Andorinhas supergroup, the Arco Verde tonalite, and the Musa granite (Fig. 1, left). A geological section across the Pedra Preta deposit shows the Musa granite emplaced into the Andorinhas supergroup rocks, as well as steeply dipping, wolframite-rich quartz veins cutting both the granite cupola at depth and the greenstone rocks at upper levels (Fig. 1, right). To the south of the Pedra Preta deposit, the veins also cross-cut the Arco Verde tonalitic rocks. Tungsten ore is characterized by a low Mn/Fe ratio and therefore has a ferberite composition.

The Arco Verde tonalite consists mainly of saussuritized plagioclase with variable amounts of amphibole, chloritized biotite, quartz, epidote, and calcite. The metamorphosed komatiites and basalt flows of the Babaçu group are composed of different proportions of amphiboles (actinolite, tremolite, and hornblende), plagioclase, biotite, chlorite, talc, quartz, and opaques, whereas the Lagoa Seca metasandstones have a granoblastic texture and mineral composition dominated by quartz, biotite, chlorite, and
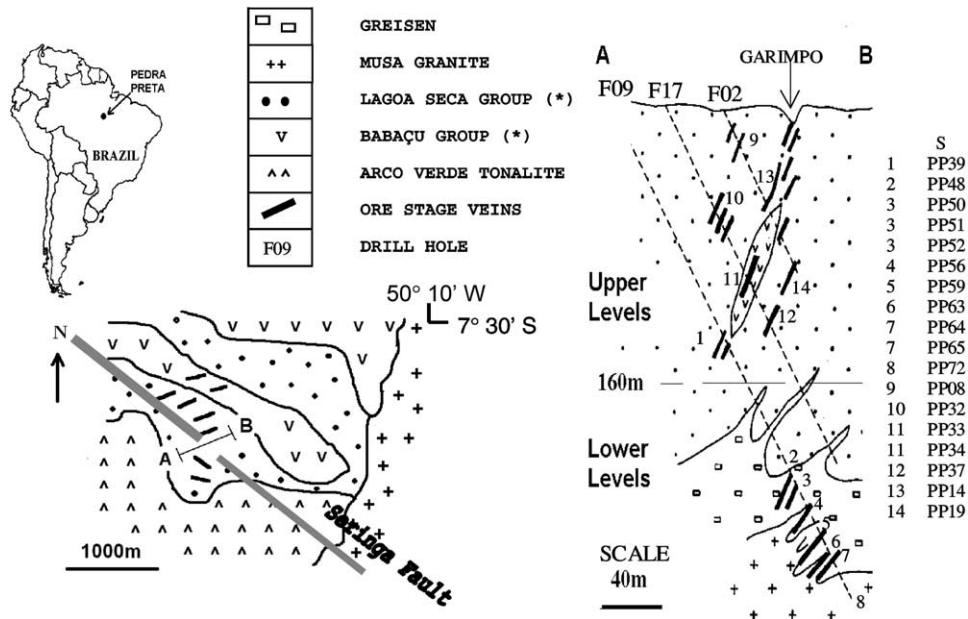
Fig. 1. Left: location and simplified geological map of the Pedra Preta wolframite deposit. Right: cross-section (A–B) of the Pedra Preta deposit (modified from Santos (1987) and Cordeiro et al. (1988)). Obs: (*)Andorinhas supergroup; GARIMPO: site of rudimental explotation of W; (1–14): sample location in drill holes; (s): sample number; F09: drill holes.

white mica. The Musa granite is formed by leucocratic, fine-grained, inequigranular rocks in which microcline, bluish quartz, oligoclase, and biotite are the main mineral constituents. Opaques, zircon, and muscovite occur in subordinate amounts. A hydrothermal overprint character-ized by the presence of topaz, fluorite, tourmaline, wolframite, and sulfides can also be observed in all lithological types of the deposit.

Three types of hydrothermal veins have been identified in the deposit. The pre-ore-stage veins (PrOSV), probably of metamorphic derivation, occur prior to the Musa granite intrusion and are hosted by the clastic units of the Andorinhas supergroup. These veins are highly deformed and consist of recrystallized quartz (>90%) and white mica. Occasionally, late topaz and sulfides are present. The second type, referred to as ore-stage veins (OSV), is related to the emplacement of the Musa granite. Initially, their formation involved the filling of fractures by quartz and wolframite (and traces of hematite; Santos, 1987), followed by reactivation and reopening of the healing fractures, which made room for the precipitation of wolframite, topaz, fluorite, and white mica. Although wolframite tends to be concentrated toward the center of the veins, it also may be randomly distributed along the veins, usually in association with topaz (Fig. 2A and B). Less frequently, wolframite occurs close to the contact with the host rocks in coexistence with quartz. Wolframite precipitation seems to have started at the final stages of OSV quartz formation but ended sometime before the fluorination process (topaz-fluorite). The third vein type comprises the post-ore-stage veins (POSV), which are rare in comparison with OSV. The POSV present a stepwise formation, including an early

precipitation of quartz, chlorite, sulfides, and carbonates followed by a late quartz deposition.

Four different quartz generations have been recognized in these veins: quartz 1 (from the PrOSV), quartz 2 (from the OSV), and quartz 3 and 4 (corresponding to early and late POSV quartz, respectively).

Wall-rock alteration is well developed around the OSV and POSV. Regardless of the host rocks, similar greiseniza-tion products can be found in the OSV haloes. The granitic rocks are bleached and partially transformed into a mass of quartz, phengite, and feldspar, with subordinate amounts of topaz, fluorite, sulfides, and titanite. Although altered to massive sericite, phengite, and chlorite, as well as occasional grains of topaz and fluorite, the greenstone rocks developed less conspicuous haloes around those veins that they hosted.

The paragenetic sequence of the Pedra Preta deposit, including both late and postmagmatic products, is presented in Table 2.

4. Fluid inclusion studies

4.1. Analytical techniques and sampling

All samples were collected from drill cores. Micro-thermometric measurements were obtained in Chaixmeca and Fluid Inc. cooling–heating stages at the Fluid Inclusion Laboratory of the Center for Development of Nuclear Technology (CDTN). The mineral identification was complemented by X-ray diffraction, and the chemical analysis for tungsten was performed by X-ray fluorescence,
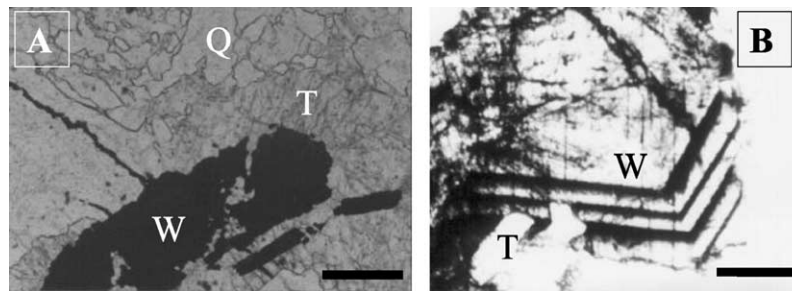
Fig. 2. Photomicrographs. (A) OSV sample of the upper part of deposit. Late topaz crystal (T) enveloping earlier wolframite (W). Q: quartz 2. Bar = 0.2 mm. (B) Wolframite crystal from OSV under IR light microscopy showing growth zones and late topaz crystals (T). Bar: 0.2 mm.

also at the CDTN. A cathodoluminescence study, carried out at the Geology Department of the Federal University of Ouro Preto (UFOP), served to highlight textural features of the vein topaz and fluorite. Volatile phases in FIs were identified by Raman microspectroscopy and infrared spectrometry at the Physics Institute of the Federal University of Minas Gerais (UFMG). Oxygen isotope determinations were obtained in a double-emission SIRA II mass spectrometer at the Stable Isotope Laboratory (LABISE) of the Federal University of Pernambuco (UFPE), following methods described by Taylor and Epstein (1962) and Sial et al. (1992). Infrared (IR) FI studies on opaque minerals were carried out using an IR emission/regulator built at CDTN with a lens operating near IR range (1000 to ≈ 1200nm). The use of IR microscopy to study FIs in opaque minerals was first described by Campbell et al. (1984) and Campbell and Robinson Cook (1987). The physico-chemical basis for IR transparency of opaque minerals can be found in Campbell et al. (1984), Richards and Kerrich (1993), Mancano and Campbell (1995), and Luders and Ziemann (1999). Synchroton X-ray fluorescence (SXRF) analyses were performed at the Syncroton Light National Laboratory (LNLS) at Campinas University.

The samples selected for analyses not only record different hydrothermal events, but also indicate that these events were distinctly imprinted on the upper and lower levels of the deposit. Samples from deeper levels present the best record of the early hydrothermal stage.

All types of quartz from different levels of the deposit have been investigated. Because quartz 2 grains are, to a lesser or greater extent, recrystallized, their more preserved areas were selected for FI studies. Compared with those in the less preserved areas, fracture planes in the more preserved areas are not common. Similar studies were carried out on quartz from the Musa granite, clastic host rocks, and veins occurring at the north of the Musa intrusion. Wolframite crystals frequently show areas with good transparency for IR microscopy (Fig. 2B), making it possible to inspect their FIs. The SXRF technique was applied to study FIs for topaz and quartz 2.

4.2. Fluid inclusion microscopy, microthermometry, Raman microspectroscopy, and synchroton X-ray fluorescence

On the basis of their modes of occurrence and phases present in the cavities, FIs were classified into four types (Table 3).

4.2.1. Type 1

These FIs are predominantly $H_2O-CO_2-CH_4$ inclusions, present irregular shapes and dimensions smaller

Table 2
Paragenetic sequence and hydrothermal alteration types in the Pedra Preta ore deposit

Alteration/ore minerals	Time (relative)		
	Pre-ore stage	Ore stage	Post-ore stage
Silicification (quartz 4)			▬▬▬
Carbonatization			▬▬▬
Sulfidation			▬▬▬
Chloritization			▬▬▬
Silicification (quartz 3)			▬▬▬
Potassic alteration			▬▬▬
F-Metasomatism (topaz and fluorite)		▬▬▬	
Wolframite		▬▬▬	
Silicification along fracture planes (quartz 2)		▬▬▬	
Microclinization (granite cupola)	▬▬▬		
Albitization (granite cupola)	▬▬▬		
Crystallization of the granite quartz	▬▬▬		
Silicification (quartz 1)	▬▬▬		

Table 3
Types of fluid inclusions from the Pedra Preta ore deposit

	Type 1 (*)	Type W	Type 2		Type 3		Type 4
Subtype			2A	2B	3A	3B	
Mineral/vein hosts	Quartz 2 (OSV), Quartz 1 (PrOSV)	Wolframite (OSV)	Topaz fluorite (OSV)	Topaz fluorite (OSV)	Quartz 3 (POSV)	Quartz 3 (POSV)	Quartz 4 (POSV)
Composition	$H_2O + CH_4 + CO_2 + NaCl + CaCl_2$ (?) Secondary (in Quartz 1), Primary (in Quartz 2)	$H_2O + CO_2 + CH_4$ (?) + salt Primary	$H_2O + CO_2 + CaCl_2 + NaCl$ Primary	$H_2O + CaCl_2 + NaCl$ Primary	$H_2O + CaCl_2 + NaCl + Li$ (?) Primary	$H_2O + NaCl + KCl$ (?) Secondary	$H_2O + NaCl$ Primary

*Also in Musa Granite quartz.

than 8 μm, and occur particularly in quartz 2 (OSV), usually along microfractures. Type 1 inclusions were recognized as secondary FIs in both the magmatic quartz (Musa granite) and quartz 1 (PrOSV veins). In the lower levels of the deposit (depths of 160–270 m), the volume fraction of the carbonic phase in these inclusions is less than 0.3 (Fig. 3A), whereas in the upper levels (depths of 25–160 m), it ranges from 0.1 to 1.0 (Fig. 3B), mostly due to necking down. Evidence of necking down is common, and stretched inclusions frequently can be observed. As a consequence, many one-phase aqueous inclusions (<5 μm) have been formed.

Microthermometry highlights the contrasts between Type 1 inclusions in samples from the lower and upper levels of the deposit. In the lower level samples, the CO_2 melting temperatures (Tm_{CO_2}) range from −60.5 to −56.6 °C (Table 4). Raman spectroscopic analyses confirm CO_2 as the main component in the carbonic phase and reveal trace amounts of CH_4 (Table 5). Methane is detected only in FI associated with late microfractures. The homogenization of the carbonic phase takes place predominantly in the liquid state at temperatures (Th_{CO_2}) between −9.5 and +28.5 °C, whereas clathrate melting temperatures (Tm_{clat}) vary from 6 to 10 °C (Table 4). In FI with $X_{CH_4} < 0.07$, as based on Tm_{clat} and with a negligible partitioning of CH_4 in the clathrate (Seitz and Pasteris, 1990), salinities are estimated at 0.67–7.3 wt% NaCl equivalent. These FIs homogenize by the disappearance of the carbonic phase at total homogenization temperatures (Th_{total}) that range from 240 to 390 °C.

In the upper level samples, Tm_{CO_2} values are much lower, ranging from −71.5 to −59 °C, because of higher CH_4 concentrations ($X_{CH_4} > 0.14$) in the carbonic phase (Tables 4 and 6). The carbonic phase homogenizes into a liquid or vapor state at highly variable negative temperatures (Table 4). Several Th_{CO_2} values are in the −30 to −64 °C range, particularly in those FI with higher CH_4 contents. In addition, approximately 30 aqueous-carbonic and one-phase carbonic inclusions indicate homogenization of the carbonic phase in the liquid state at very low temperatures (−90 to −82.5 °C). Solid CO_2 melting was not observed in the inclusions. Th_{clat} measurements fall between 10 and 16 °C. Raman spectroscopy indicates that CH_4 is the sole component of the carbonic phase in the inclusions. In a few FI, the laser beam forms a dark solid phase, which suggests the presence of other hydrocarbons. The Th_{total} distribution of the aqueous-carbonic inclusions (both lower and upper levels) spreads over the 220–390 °C range (Table 4), with higher frequencies between 220 and 310 °C (Fig. 4). During heating runs, approximately 5% of the FI decrepitated. Eutectic temperatures (T_{EU}) of the aqueous phase at −52 °C suggest that Na^+ and Ca^{++} are the main cations in solution. Carbonate daughter minerals detected by Raman spectroscopy can frequently be seen.
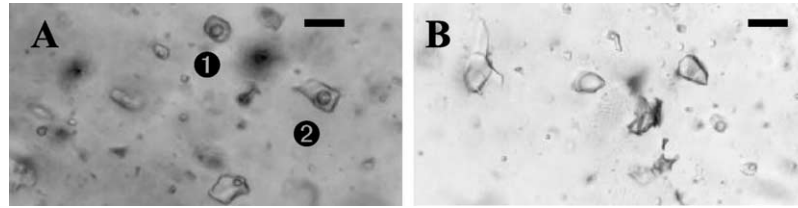
Fig. 3. Photomicrographs. (A) Quartz 2 FI from the lower part of the deposit (OSV cutting Musa granite cupola). Early aqueous-carbonic FI (Type 1) are shown (ex: 1,2). Micro-Raman analyses indicate pure CO_2 for the carbonic phase. Bar: 10 μm. (B) Quartz 2 aqueous-carbonic (Type 1) FI of the OSV from upper part of the deposit. Micro-Raman analyses indicate $CH_4 + CO_2$ for the carbonic phase. Scale bar: 10 μm.

4.2.2. Type W

These FI were studied in wolframite crystals from the OSV (upper part of the deposit). They are tube-like, two-phase (L + V), aqueous-carbonic inclusions, with sizes reaching 15 μm. The vapor phase occupies up to 30% of their volume (Fig. 5A).

During freezing runs, no phase changes, which are indicative of the presence of N_2 or carbonic compounds, were observed. On warming, however, the bubble underwent deformation around −30 °C and recovered its original shape only between +5 and +5.5 °C, which indicates clathrate formation and, therefore, the presence of trace amounts of carbonic or N_2 phases. These FI homogenize in the liquid state at Th_{total} between 270 and 336 °C.

4.2.3. Type 2

This type was identified in topaz and fluorite crystals from OSV. They are primarily aqueous-carbonic (subtype 2A) and aqueous (subtype 2B) inclusions and display sub-rounded to irregular shapes and dimensions from 4 to 50 μm (Fig. 5B). Their degree of filling ranges from 0.4 to 0.7 in topaz and is below 0.4 in fluorite grains. Carbonate daughter crystals are eventually found in these inclusions.

The subtype 2A aqueous-carbonic inclusions contain an aqueous phase with salinities of 7–8 wt% NaCl equivalent, as inferred from the Tm_{clat} (6–6.5 °C), and a carbonic phase of solely CO_2, in agreement with a Tm_{CO_2} of −56.6 °C. Th_{CO_2} values are in the 28–31.3 °C range (Table 4), and homogenization occurs in the vapor state. Th_{total} values vary from 240 to 390 °C (Fig. 4) but are more frequently between 310 and 360 °C in topaz and at 240 °C in fluorite. Total homogenization is marked by the disappearance of the aqueous phase.

In the subtype 2B aqueous inclusions, salinities of 9.5–14 wt% NaCl equivalent were estimated from their ice melting temperatures (Tm_{ice}). Again, the presence of Ca^{++}

and Na^+ is inferred from T_{EU} values of −50 to −47 °C. Th_{total} values are concentrated mainly between 280 and 380 °C, and homogenization takes place in the liquid state. The SXRF analyses detected not only Ca^{++}, but also Si, Ti, Cu, and Mn in the fluids.

4.2.4. Type 3

This type includes primary and secondary, one- and two-phase inclusions trapped in quartz 3 from the POSV. The primary FI are small (<10 μm) and present pseudopolygonal outlines with a very low degree of filling (0.1–0.2) (Fig. 5C); the secondary FI are even smaller. They are referred to as subtypes 3 A (primary) and 3B (secondary). In addition to a vapor phase, some of them may contain rectangular-shaped daughter minerals, tentatively identified as carbonates by Raman microspectroscopy.

Primary 3A subtype FI shows T_{EU} varying from −45 to −52 °C, with most values clustering between −48 and −52 °C, which suggests the presence of $CaCl_2$ in solution. In POSV samples collected at a depth of 270 m, the FI show positive salt hydrate dissociation temperatures (Tm_H) that range from 10.2 to 19.5 °C (Table 7). In these FI, a recrystallization was noted at 25 °C, but no ice melting was observed. These measurements point to $CaCl_2$-rich fluids and indicate that the salt hydrate is antarcticite. Accordingly, salinities could be estimated at 34–36 wt% $CaCl_2$ equivalent (Fuzikawa, 1982, 1985). Samples collected at a depth of 60 m contain 3A subtype FIs with similar T_{EU}, but no hydrate is observed. Instead, ice crystals are the last to melt at temperatures between −19 and −8.3 °C, thereby allowing the salinities to be estimated at 12–20 wt% $CaCl_2$ equivalent. Moreover, similar 3A subtype FIs are present in OSV quartz 2 crystals at the same depth (60 m), but they differ in that they have T_{EU} values in two distinct intervals: −57 to −50 °C and −72 to −70 °C. The lower temperature interval may indicate the presence of dissolved cations other

Table 4
Microthermometric data for the aqueous-carbonic fluids (Types 1 and 2) related to the Pedra Preta deposit

IF type	Mineral	Tm_{CO_2}	Th_{CO_2}	Tm_{clat}	Th_{total}
1 (upper levels)	Quartz 2 (OSV), Quartz 1 (PrOSV)	−71.5 to −59, $n = 36$	−90 to 16, $n = 84$	10–16, $n = 33$	220–390, $n = 70$
1 (lower levels)	Quartz 2 (OSV)	−60.5 to −56.6, $n = 31$	−9.5 to 28.5, $n = 64$	6–10, $n = 37$	240–390, $n = 40$
2	Topaz fluorite (OSV)	−56.6, $n = 41$	28–31, $n = 50$	6–6.5, $n = 35$	240–350, $n = 42$

Tm_{CO_2}: carbonic phase melting temperature (°C); Th_{total}: total homogenization temperature (°C); Tm_{clat}: clathrate melting temperature (°C); Th_{CO_2}: carbonic phase homogenization temperature (°C); and n: number of measurements.

Table 5
Chemical composition of selected Type 1 aqueo-carbonic fluid inclusions in quartz 2 (from lower level OSV)

Sample	Fill	Microthermometry data (°C)				Composition of the non aqueous phase (1)			NaCl% (2)	Obs
		Tm_{CO_2}	Tm_{clath}	Th_{CO_2}	Th_{total} (°C) (3)	d_{CO_2}	X_{CO_2}	X_{CH_4}		
PP25-1-1	0.2	−57.5	7.0	23.0 (L)	300	0.71	0.98	0.01	5.6	
PP25-1-2	0.3	−56.9	8.0	5.0 (L)	246	0.88	0.99	0.009	4.7	
PP65-5-3	0.4	−58.4	7.7	21.8 (L)	288	0.60	0.92	0.07	4.4	
PP65-5-4	0.3	−58.0	8.6	22.5 (L)	271	0.63	0.94	0.05	2.76	
PP65-5-5	0.3	−58.0	8.0	18.0 (L)	290	0.72	0.94	0.05	3.89	
PP65-7-1	0.3	−58.3	7.5	16.4 (L)	305	0.73	0.94	0.05	4.79	
PP70-2-1	0.2	−56.8	7.0	28.0 (L)	280	0.65	0.99	0.003	5.6	
PP70-2-3	0.3	−56.6	8.0	27.5 (L)	241	0.66	1.0	–	3.9	
PP70-3-1	0.2	−56.6	7.5	28.0 (L)	246	0.65	1.0	–	4.7	
PP70-3-2	0.2	−56.6	8.0	27.8 (L)	251	0.66	1.0	–	3.9	
PP70-3-4	0.2	−56.6	7.7	27.1 (L)	260	0.67	1.0	–	4.4	
PP70-4-4	0.2	−56.6	7.9	27.6 (L)	282	0.66	1.0	–	4.0	
PP70-5-1	0.3	−56.6	8.2	27.9 (L)	260	0.65	1.0	–	3.5	
PP70-5-2	0.2	−56.6	8.0	28.5 (L)	265	0.64	1.0	–	3.9	
PP70-5-3	0.3	−56.6	8.1	26.0 (L)	252	0.69	1.0	–	3.7	
PP70-5-4	0.3	−56.6	7.6	26.1 (L)	277	0.70	1.0	–	4.6	
PP71-2-1	0.2	−57.0	8.0	22.6 (L)	266	0.72	0.98	0.01	3.9	
PP71-2-2	0.2	−56.9	8.1	27.0 (L)	244	0.66	0.99	0.009	3.7	
PP65-4-3	0.9	−59.0	7.1	21.8 (L)	290	0.40	0.87	0.12	5.6	(4)
PP65-5-1	0.7	−57.8	7.1	21.0 (L)	–	0.75	0.98	0.01	5.5	(4)
PP71-2-3	0.8	−57.8	7.4	27.0 (L)	282	0.46	0.95	0.046	4.9	(4)
PP71-2-4	0.9	−57.5	7.4	24.0 (L)	–	0.67	0.96	0.03	4.9	(4)

Tm_{CO_2}: CO2 melting temperature; Tm_{clath}: clathrate melting temperature; Th_{CO_2}: CO2 homogenization temperature; d_{CO_2}: density of carbonic phase; Th_{total}: total homogenization temperature; L = liquid; V = vapor; (1) composition of the nonaqueous phase was determined using MacFlincor 0.9 software, Raman microprobe data, and Origin 5.0 software; (2) NaCl% salinity (wt% NaCl equiv.); (3) FI homogenized into the CO2 phase; (4) Type 1 FI from or near fracture planes.

than Ca^{++} (Li+?) or metastability (see Section 4.2.5). Regardless of the T_{EU} differences, all inclusions yield the same Tm_{ice} (−28 to −24 °C) and therefore the same salinities (22–25 wt% CaCl2 equivalent). As a whole, the 3A subtype FIs homogenize into the liquid state between 140 and 220 °C (Table 7).

Samples from a quartz vein that crops out at the northern border of the Musa granite, 12 km from the Pedra Preta deposit, were also studied. Primary aqueous FIs on quartz crystals are similar to the 3A subtype. Their T_{EU} is approximately −68 °C, whereas the Tm_{ice} varies from −34.7 to −33.3 °C, thereby indicating a salinity of

Table 6
Chemical composition of some Type 1 aqueous-carbonic fluid inclusions in quartz 2 from upper level OSV

Sample/inclusion number	Fill	Microthermometry (°C)			Composition of non-aqueous phase[1]				Obs
		Tm_{CO_2}	Tm_{Clath}	Th carbonic phase	CO2		CH4		
					MF	Peak	MF	Peak	
PP03-q-1-1	0.6	−59.5	15.1	−4.1 (L)	79.17	1384.6	20.76	2909.8	H2S < 0.1
PP03-q-1-6	0.4	−64.0	14.0	−35.0 (L)	46.7	1385.2	53.3	2911.3	
PP03-q-1-7	0.5	−60.3	11.5	−19.0 (L)	80.8	1385.2	19.12	2911.3	
PP03-q-1-8	0.4	−58.7	13.0	−6.0 (L)	81.0	1386.3	19.0	2911.3	
PP22-q-6-1	0.2	−71.5	–	−55.0 (L)	24.0	1384.5	76.0	2909.6	
PP22-q-9-1	0.4	−61.8	–	8.9 (V)	82.3	1383.5	17,7	2909.4	
PP22-q-9-2	0.9	−60.8	–	0.4 (L)	86.0	1384.2	14	2909.7	
PP22-q-9-3	0.7	−62.1	–	5.9 (V)	78.7	1384.3	21.3	2909.5	
PP21-1-1	0.8	−60.2	–	−10 (L)	65.3	1385.1	34.7	2910.9	
PP21-1-2	1.0	−67.5	–	−53.5 (L)	13.8	1385.1	86.5	2910.9	
PP21-1-3	1.0	−69.5	–	−60.2 (L)	–	–	–	–	(2)

Tm_{CO_2} = CO2 melting temperature; Tm_{clath} = clathrate melting temperature; L = liquid; V = vapor; (1) composition of the nonaqueous phase was determined using MacFlincor 0.9 software, Raman microprobe data, and Origin 5.0 software; (2) strong luminescence prevented CO2 and CH4 Raman spectra; MF = molar fraction.
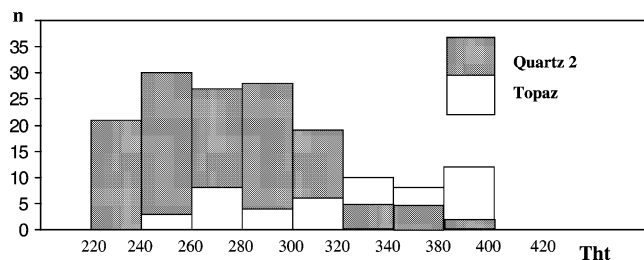
Fig. 4. Histogram showing total homogenization temperatures of Type 1 (quartz 2) and Type 2 (topaz) FI from OSV. Tht: total homogenization temperature (°C); n: number of measurements.

approximately 27 wt% $CaCl_2$ equivalent. Aqueous FIs with a similar composition and morphology were studied in magmatic quartz from the Musa granite collected 2 km east of the deposit.

During freezing tests of 3B subtype inclusions of POSV quartz trapped along trails, the disappearance of isotropic grains with a cubic habit and the formation of an ice and salt hydrate (hydrohalite?) are notable. The hydrate dissociates incongruently, forming a cubic mineral between 0 and 15 °C. This behavior is a strong evidence of the metastable dissociation of hydrohalite in fluids with salinities over the $H_2O-NaCl$ eutectic composition. Accordingly, on heating, the halite crystals dissolve between 180 and 194 °C, thus implying a brine with 30 wt% NaCl equivalent (Bodnar and Vityk, 1994).

4.2.5. Type 4

This population is interpreted as primary aqueous inclusions trapped in quartz 4 crystals that represent the last generation of quartz formed in the deposit. In quartz 2 and 3, these FIs appear as subordinate, secondary cavities. Some one-phase inclusions nucleate a bubble during cooling, which does not disappear they are heated back to room temperature, which indicates typical metastable behavior of the fluid. T_{EU} occurs around -22 °C, thus suggesting that the solution is Na-rich and that Ca^{++} cations are unimportant. Salinities of 1.2–4.2 wt% NaCl equivalent are estimated from Tm_{ice} measurements (-2.5 to -0.7 °C). Homogenization takes place into the liquid state at <150 °C.

4.3. Interpretation of the FI data

Many compositional differences were observed in Type 1 inclusions in quartz 2 from the lower and upper levels of the deposit. At the lower levels, in preserved areas of quartz 2, Type 1 aqueous-carbonic FIs, distant from microfractures or recrystallized zones, have a carbonic phase that consists of almost pure CO_2 and an aqueous phase of low salinity (<7 wt% NaCl equivalent). The coexistence of very small (<5 μm) CO_2-free aqueous inclusions associated with inclusions of aqueous-carbonic composition is interpreted as a result of necking down or heterogeneous trapping. However, Type 1 FIs, trapped in the upper level quartz 2, contain low salinity aqueous-carbonic solutions, but the CH_4 concentrations are higher, even surpassing CO_2 concentrations in a few cases.

To explain the formation and composition of Type 1 FI, the following points should be taken into account:

1. Type I FIs from the upper levels present both the degree of filling and the CH_4 contents of the highly variable carbonic phase. Those FIs away from fracture surfaces are often oriented. In contrast with the lower levels, the association of aqueous and aqueous-carbonic FI was not observed. The carbonic phase of the FI hosted by late fractures has variable CH_4 and CO_2 contents ($CH_4 \gg CO_2$);
2. The Pedra Preta deposit is located within the influence of the Seringa fault zone;
3. CH_4 is seldom of magmatic origin, particularly if it occurs in high concentrations. It is uncommon to find significant amounts of this gas in silica supersaturated granitoid fluids (Roedder, 1984; O'Reily et al., 1997);
4. In quartz 2 from the lower levels, CH_4 occurs only in fracture-controlled FI and in trace amounts;
5. Fluids associated with greenstone rocks are generally highly charged with CH_4; and
6. The range of T_H is highly variable.

On the basis of these considerations, a model for the evolution of the fluid regime at the Pedra deposit, represented by the investigated FI, is proposed.

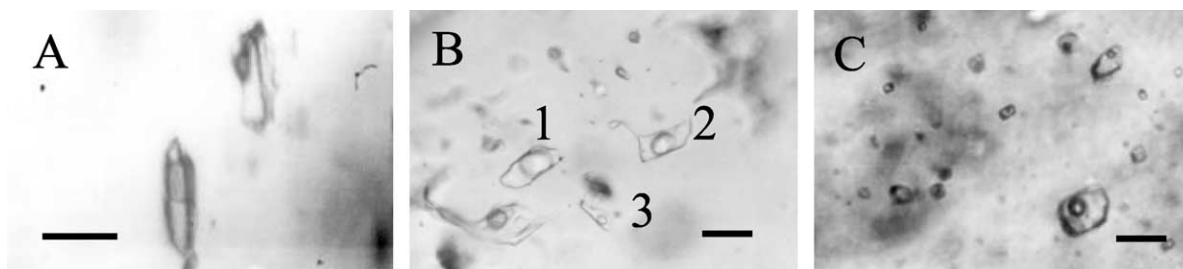Late granitic fluids, probably aqueous-saline with traces of CO_2, may have interacted with reducing, CH_4-rich,

Fig. 5. Photomicrographs. (A) Type W two phase primary aqueo-carbonic FI in wolframite crystal (OSV) under IR light. Bar: 10 μm. (B) (1,2,3): Type 2 aqueo-carbonic primary FI in topaz (OSV). Bar: 10 μm. (C) Primary Type 3A FI in quartz 3 (POSV). Bar: 10 μm.

Table 7
Microthermometric data of types 3 and 4 aqueous fluid inclusions

IF type	Mineral	T_{EU} (°C)	Tm$_{ice}$ (°C)	Tm$_H$ (°C)	Ts (°C)	Th$_{total}$ (°C)
3A	Quartz 3	− 48 to − 52, $n = 20$		10.2–19.5 (anctarticite?), $n = 14$		140–220, $n = 65$
3B	Quartz 3			0–15 (hydrohalite?), $n = 12$	180–194, $n = 14$	130–150, $n = 32$
4	Quartz 4 (?)	− 22, $n = 11$	− 2.5 to − 0.7, $n = 56$			>100, $n = 61$

T_{EU}: Eutectic temperature; Tm$_{ice}$: ice melting temperature; Tm$_H$: hydrate melting temperature: Th$_{total}$: total homogenization temperature: Ts: halite dissolution temperature.

greenstone-derived fluids. A convecting system set forth by the cooling of the Musa granite led to the mixing of magmatic and metamorphic fluids by the time the OSV veins formed. At the upper levels, fluids highly enriched in CH_4 were trapped as primary FI in quartz 2, whereas at the lower levels—as a consequence of higher O_2 fugacity conditions imposed by the oxidizing Musa granite (Magalhães and Dall'Agnol, 1992)—CO_2 could have formed as a product of the CH_4 oxidation (Fig. 6). That is probably why CH_4 is absent in FI in quartz 2 away from fractures.

The OSV from the upper levels were formed in greenstone host rocks, which were already sheared because of movements of the Seringa lineament. Thus, later fracturing caused quartz 2 crystals to be broken at all levels of the deposit, which allowed the percolation of reducing, CH_4-rich fluids and the trapping of secondary FI, some of which were pure methane. The shear zones remained active, forming microdislocations in quartz 2 that oriented the primary FI and may have favored necking down and oxidation of CH_4. This process would explain the extremely variable CO_2 contents found in secondary FIs that occur along fracture surfaces at the upper levels. At the lower levels, in turn, the greater mechanical resistance of the granitic rocks to deformation may have prevented the primary FI from being modified, thus preserving the composition.

In this context, the granite-derived late-stage fluid can be assumed to have been a moderately saline aqueous solution with Cl^-, Na^+, and subordinate amounts of dissolved carbonic compounds. Necking down along those planes may have formed FIs with variable carbonic phase volume fractions, among them one-phase carbonic inclusions. It also may be responsible for the dispersion of T_{ht} obtained in
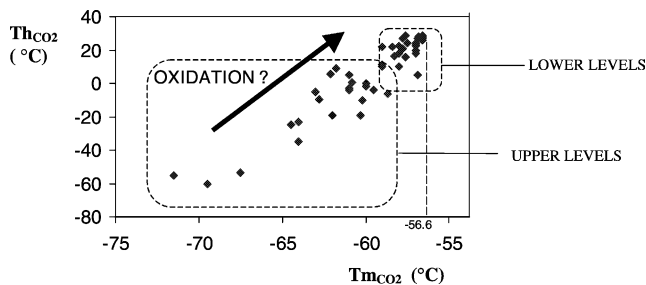

Fig. 6. Th$_{CO_2}$ vs. Tm$_{CO_2}$ diagram showing compositionally different primary Type 1 fluid inclusions in the upper and lower levels of the Pedra Preta deposit. The trend indicates higher CO_2/CH_4 ratios.

OSV quartz. Therefore, only Type1 inclusions in preserved areas of quartz 2 from the lower levels have been used for pressure estimates. These unmodified FIs likely are the best representative samples of the magmatic hydrothermal fluids that formed the OSV at the greisenized cupola of the Musa intrusion.

Primary FIs in wolframite show similarities with Types 1 (quartz) and 2 (topaz). Although clathrates can be detected, no Type W FIs present typical phase changes of carbonic compounds during freezing runs, as the topaz primary aqueous-carbonic inclusions do. Crushing tests of wolframite grains immersed in glycerine and kerosene reveal moderate gas release, which implies the presence of gases under pressure in the FI. The released bubbles dissolve slowly in kerosene, but a few dissolve more rapidly, probably due to the trace amounts of CH_4 in the fluid. Spectrometric IR analyses of wolframite crystals confirm the presence of CO_2. These data suggest that wolframite was precipitated from a low to moderate saline, predominantly aqueous fluid that contained some CO_2 ($X_{CO_2} \approx 0.1$) and trace amounts of CH_4. Compositionally, this fluid is similar to Type 1 aqueous-carbonic solutions from the upper levels of the deposit. The low CO_2 contents, however, may reflect mixing of the metamorphic fluids with larger volumes of granite-derived aqueous solutions or, alternatively, no mixing and the precipitation of wolframite from essentially magmatic aqueous solutions.

After most of the quartz 2 was deposited, wolframite and hematite precipitated in response to an increase in the oxygen fugacity, which caused a progressive rise in the CO_2 concentrations of the regional fluids, possibly by means of the reaction $CH_4 + O_2 \Leftrightarrow CO_2 + H_2O$. According to Santos (1987), quartz 2 started forming long before it coprecipitated with wolframite and hematite. Petrographic evidence in this study shows that some wolframite crystals contain quartz 2 inclusions, but those associated with topaz are quartz-free. This indicates that wolframite precipitation coincides only partially or postdates quartz 2 formation. Compositionally distinct FIs trapped in quartz 2 and wolframite grains corroborate this interpretation.

Fluorine metasomatism subsequent to the wolframite precipitation is represented by the crystallization of topaz (Fig. 2B) and fluorite. There was a large temperature overlap during the precipitation of quartz 2, topaz, and wolframite. CO_2 concentrations decreased progressively, which rendered the fluorite-forming fluids poorer in CO_2

($X_{CO_2} < 0.1$) compared with those that were precipitating topaz. The large variation in the degree of filling of type 2 FI is here interpreted as a result of the immiscibility of a supercritical aqueous-carbonic fluid during cooling that contained Ca, Na, Si, Ti, Cu, and Mn. Necking down plays a subordinate role.

Quartz 3 of the POSV was formed in a CO_2-free environment from a $CaCl_2$-rich, aqueous fluid with an estimated salinity of 36 wt% $CaCl_2$ equivalent, obtained in primary FI in quartz 3 from the lower levels. At the upper levels, the fluid salinity is lower, which implies a dilution of the magmatic fluids as they moved upward. Type 3 inclusions from both the deposit and the quartz vein that crops out at the northern border of the Musa granite display a remarkably low T_{EU} (≈ -60 to $-70\,°C$). These values are considered metastable T_{EU} of the $NaCl-CaCl_2-H_2O$ system (Davis et al., 1990) or due to the phase transitions of hexagonal ice in fluids of identical composition (Walker and Samson, 1998). The presence of Li and Sr in the fluids also could produce similar results (Oakes and Bruce, pers. comm.). Both elements are expected in a granite-derived aqueous solution.

As the temperature dropped below $200\,°C$, restricted circulation of NaCl (and probably KCl) saturated solutions, thus forming the 3B subtype inclusions. The last stage of silica precipitation (quartz 4), corresponding to Type 4 FI, occurred below $150\,°C$ and probably under hydrostatic pressures. The differences in salinities and densities among 3A, 3B, and 4 FI types are likely due to their distinctive origins. Type 3A FI may represent last-stage magmatic fluids enriched in $CaCl_2$. Ca was probably provided, at least in part, by the alteration of amphiboles of the greenstone rocks and plagioclase of both greenstone rocks and greisenized granite. The 3B inclusions, in contrast, may represent connate waters or deep groundwater enriched in Ca^{+2} and Na^+, similar to those found in the Canadian shield (Frape and Fritz, 1987; Guha and Kanwar, 1987). Finally, Type 4 inclusions may represent fluids with some contributions from near-surface waters.

5. Oxygen isotope studies

Oxygen isotope studies were carried out on quartz from the Musa granite, as well as on quartz, wolframite, and phengite from the OSV (Rios et al., 1998). Quartz from both the granite and OSV from lower levels show similar isotopic compositions ($\delta^{18}O_{quartz} = 7-8‰$ SMOW), which indicates isotopic equilibrium with a common fluid. Conversely, quartz of the OSV from the upper levels have $\delta^{18}O_{quartz}$ in the $9.0-9.7‰$ SMOW range. This difference of up to $2.7‰$ between the lower and upper levels cannot be attributed solely to temperature, because microthermometric data record the same thermal interval ($250-350\,°C$) for the whole vein. The distinct $\delta^{18}O_{quartz}$ ranges may reflect the oxygen isotopic composition of the dominant lithological

varieties in the lower (granitic rocks) and upper (metamafic and metasedimentary rocks) levels with which the fluids have interacted. Equally significant may be the compositional differences of the aqueous-carbonic fluids that circulated in the upper (CH_4-enriched) and lower (CO_2-enriched) levels. Partitioning of ^{18}O is more favored in fluids with CO_2 relative to those in which this gas is absent (e.g. Higgins, 1985a,b; So and Yun, 1994).

$\delta^{18}O$ values of 0.85 and 5.44‰ SMOW are recorded for wolframite and phengite, respectively. Despite the slight alteration of wolframite to scheelite along the microfractures, quartz-wolframite, instead of wolframite-phengite, was used to calculate temperatures because it allows a larger isotopic fractionation and consequently may be considered a more sensitive geothermometer (Shieh and Zhang, 1991). An equilibrium temperature of $320\,°C$ was obtained for values of $\delta^{18}O_{quartz} = 9.04‰$ SMOW and $\delta^{18}O_{wolf} = 0.85‰$ SMOW on the basis of the $1000\ln\alpha$ curves for the quartz-wolframite pair (Shieh and Zhang, 1991). This temperature is within the $300-400\,°C$ range, beyond which W solubility decreases dramatically (Jaireth et al., 1990).

6. Pressure estimates

Pressures for the OSV quartz formation were calculated using early CO_2 pure aqueous-carbonic inclusions from the deposit's lower levels. The isochores corresponding to the PP70-5-1 and PP70-3-2 inclusions (Table 5) define the density field for the whole Type 1 FI population. At a temperature of $320\,°C$ (quartz-wolframite geothermometer), a pressure range of $2-2.75$ Kbar is constrained on the basis of the $NaCl-CO_2-H_2O$ system. Petrological studies of the Jamon granite, which is found near the Pedra Preta deposit and has the same age and mineral composition as the Musa granite (Gastal, 1987), point to pressures of approximately 3 Kbar at the final stage of crystallization history (Dall'Agnol et al., 1999a), in good agreement with the values found for the OSV veins.

$H_2O-CaCl_2$ aqueous inclusions with a density of 0.83 g/cm^3, salinity of 9.8 wt% equivalent $CaCl_2$, and negligible amounts of CO_2 were used for pressure estimates of Type 2 FI in topaz. For temperatures of $320\,°C$ (wolframite precipitation) and higher (Th$_t$ of aqueous inclusions with traces of CO_2), pressures are estimated at approximately 1 Kbar. This value indicates that fluorite precipitation occurred in pressure conditions lower than those for the crystallization of quartz 2. However, if a temperature of $380\,°C$ (Fig. 7) was considered for the onset of the fluorine metasomatism, both quartz 2 and topaz could have been deposited, at least in part, in similar pressure conditions.

Finally, the unavailability of an independent geothermometer did not permit a more precise calculation of the trapping pressure of the 3A subtype inclusions.
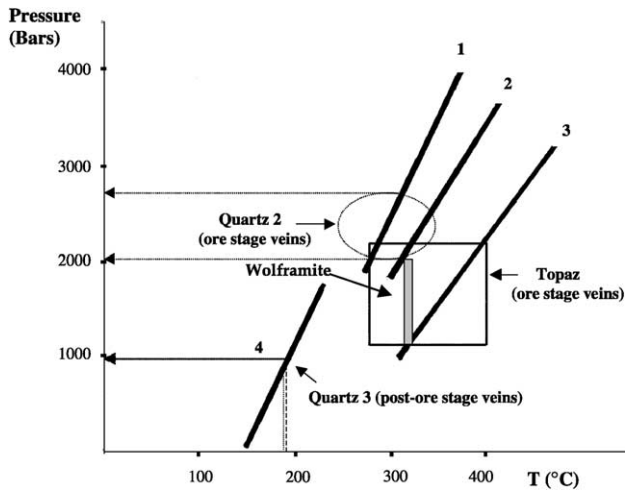
Fig. 7. Pressure–temperature diagram for fluids studied in the Pedra Preta system. (1) Fluid 1 isochore (FI PP70-3-2, quartz 2, OSV, lower level), CO_2 density = 0.66 g/cm³; (2) Fluid 1 isochore (FI PP70-5-1, quartz 2, OSV, lower level), CO_2 density = 0.65 g/cm³; (3) Fluid 2 isochore ($H_2O + CaCl_2$, topaz, OSV), fluid density = 0.83 g/cm³; (4) Fluid 3B isochore ($H_2O + NaCl$ + halite), fluid density = 1.16 g/cm³, Th = 150 °C ,Ts = 190 °C.

Nevertheless, a < 1 Kbar value has been obtained for 3B subtype inclusions that contain halite crystals. These pressure determinations followed the method used by Baker (1998) in the Eloise Cu–Au deposit brines. Therefore, only halite-bearing inclusions with salinities of approximately 30 wt% equivalent NaCl were used in the calculations. The isochore is drawn for a partial homogenization temperature of 150 °C (disappearance of the vapor phase), and the minimum pressure is estimated at 190 °C (halite dissolution).

7. Source of tungsten in the Pedra Preta deposit: magmatic or metamorphic?

Studies carried out in the past 30 years have demonstrated that tungsten transport in mineralizing solutions takes place as tungstate ion, sodium tungstate, tungstic acid, or heteronuclear acid (Krauskopf, 1967; Bernard et al., 1990). Tungstic acid is the dominant species above 400 °C, whereas at lower temperatures, HWO_4^- and WO_4^{-2} are the most stable complexes (Krauskopf, 1967, 1974; Higgins, 1985a; Wood and Vlassopoulos, 1989; Jaireth et al., 1990). Because of the common occurrence of carbonic fluids associated with tungsten deposition, other authors have suggested carbonate and bicarbonate complexes as important tungsten-transporting agents (Higgins, 1980, 1985a; Giuliani, 1984; Quilez et al., 1989; Gumiel et al., 1989). In contrast, Wood and Samson (2000) state that carbonates (together with chlorides, fluorides, and phosphates) play a negligible role in hydrothermal tungsten transport. These experimental studies indicate that wolframite is capable of

attaining solubilities of up to a thousand parts per million as H_2WO_4, HWO_4^-, and WO_4^{-2} simple tungstate species and alkali tungstate ion pairs (Wood and Samson, 2000). High tungsten solubility can also be obtained in pure water and becomes higher as f_{O_2} decreases (below the $WO_3–WO_2$ buffer), probably due to W^{+5} species formation (Wood and Vlassopoulos, 1989). Therefore, it seems that tungsten can be transported in various types of aqueous solutions in many different conditions.

Previous studies on other wolframite and scheelite deposits have indicated the dominance of an aqueous phase, followed by CO_2 and minor amounts of CH_4 and N_2 in the W-bearing solutions. These solutions are usually of low salinity, acid pH, variable temperature (100–650 °C), and oxygen fugacity ($10^{-35}–10^{-25}$ bar), and they precipitate tungsten ore at pressures of < 2.5 Kbar (Naumov and Ivanova, 1971; Higgins, 1980; Roedder, 1984; Cheilletz, 1984; Gerstner et al., 1989; Wood and Vlassopoulos, 1989; Durisova et al., 1992; Kilias and Konnerup-Madsen, 1997; O'Reily et al., 1997; Wood and Samson, 2000). The data obtained for the Pedra Preta deposit (thermal conditions of 250–350 °C, pressure about 2 Kbar, and oxygen fugacity of $10^{-38}–10^{-37}$ bar) fit within this framework.

Regardless of the composition and derivation of the fluids, the following aspects should be considered to explain the wolframite precipitation at the Pedra Preta deposit:

1. Quartz 2 precipitated from a residual magmatic aqueous-carbonic fluid, whereas topaz precipitated from a compositionally similar fluid with lower CO_2 density;
2. Temperature remained relatively constant throughout quartz 2 and topaz deposition;
3. By the time topaz started precipitating, the mineralizing fluids were largely depleted in CH_4 (FI in topaz crystals contain no other carbonic phase but CO_2);
4. A change occurred from reducing to oxidizing conditions, as suggested by the coprecipitation of hematite and wolframite; and
5. The abundance of Fe-rich minerals is much greater in the upper level rocks than in the lower level ones.

According to the FI data, two kinds of fluids could account for the transport and precipitation of tungsten at the Pedra Preta deposit:

1. A CO_2-bearing saline aqueous fluid derived from de Musa granite crystallization; or
2. A CH_4-rich aqueous-carbonic fluid, probably metamorphic, which may have been in equilibrium with the greenstone host rocks at the time of the granitic intrusion.

The following arguments favor W transport by metamorphic fluids:

1. Crushing tests in wolframite suggest the presence of CH_4 in the carbonic phase of the trapped fluids, making them

compositionally similar to Type ii reducing metamorphic fluids;

2. Although the W mineralization is assumed to have little dependence on the redox state of the magma (Blevin and Chappell, 1992), it is normally associated with granites of the ilmenite series (Ishihara, 1981; Sillitoe, 1996). In this regard, the Musa granite is interpreted to have evolved from an oxidized magma, characterized as an A-type granite of the magnetite series (Magalhães and Dall'Agnol, 1992; Dall'Agnol et al., 1999a,b);

3. CH_4 is a volatile expected in reducing magmas that give rise to S-type granitoids (Ishihara, 1981);

4. CH_4 in the fluids was largely transformed into CO_2 ($CH_4 + 4O_2 = CO_2 + 2H_2O$) during oxidation, as evidenced by FI and mineral paragenetic data; and

5. Geochemical studies indicate the unspecialized character of the Musa granite facies associated with the Pedra Preta deposit (Gastal, 1987; Rios, 1995).

These metamorphic fluids may have been able to extract W from the rocks through which they percolated and transport it as W^{+5} ions soluble in very low f_{O_2} fluids (Wood and Vlassopoulos, 1989). The W deposition might have occurred at sites where f_{O_2} was sufficiently high to produce CO_2 at the expense of CH_4. At equilibrium, these f_{O_2} are estimated at 10^{-38}–10^{-37} bar at a temperature of 300 °C (Rios, 1995).

In support of the magmatic derivation of the W-transporting fluids, there is the geological framework of the deposit, which shows greisenized rocks in the granite cupola and, to a lesser extent, in the immediate host rocks (Fig. 1). A similar picture has been described in other deposits where W is genetically associated with granites, such as Panasqueira, Portugal (Noronha et al., 1992). Sn–W specialized granites have W contents of 3–60 ppm (Higgins, 1985a; Polya, 1989; Marignac and Cuney, 1991), though, away from the ore zone, W-mineralized granitoids are not enriched in this metal (Derré et al. in Marignac and Cuney, 1991). At the Pedra Preta deposit, X-ray fluorescence and ICP analyses of greenstone and granitic rocks do not reveal any significant W concentrations. The metasandstones have WO_3 contents of 0.05% (Docegeo, 1984; Santos, 1987), and the metavolcanic rocks and metatonalites have less than 0.1% (Docegeo, 1984). Granite samples systematically show W concentrations below the detection limit (15 ppm).

Although most arguments favor a metamorphic origin for the mineralizing fluids, the Musa granite cannot be ruled out as an alternative source for W. Even though no W was detected by synchroton XRF analyses in topaz-hosted FIs and though its deposition preceded the fluorine-rich submagmatic stage (topaz + fluorite + low density fluid composed of $H_2O + NaCl + CO_2$), some W could have been supplied by a late, more specialized granite facies not mapped yet in the deposit area. This facies would be similar

to those already described in the batholith, with fluorite contents of up to 0.8% (Gastal, 1987).

Progressive CO_2 loss following immiscibility, retrograde boiling, dilution, and pH changes of the fluids have been considered triggering factors for wolframite precipitation (Giuliani, 1984; Higgins, 1985a; Ramboz et al., 1985; Schwartz and Surjono, 1990; Slov'ev, 1990; Fernandez, 1991). At the Pedra Preta deposit, it was not possible to find evidence of these processes during the time elapsed between quartz 2 and topaz precipitation. However, two factors may have been decisive for the W deposition:

1. Lithologic-structural control—the deposit host rocks are cut by fractures related to the Seringa lineament. W-bearing solutions may have used these fractures as channelways, moving toward the upper levels of the deposit, where rocks with abundant Fe-rich minerals are common (Babaçu group). At the lower levels, where wolframite is relatively rare, rocks with expressive amounts of Fe-rich minerals are scarce.

2. Chemical control—the oxidation of CH_4-rich reducing fluids near the Musa granite.

8. Ore deposit model and concluding remarks

At least four hydrothermal events have been identified in the Pedra Preta deposit area. The first is related to metamorphic processes involving the Andorinhas super-group rocks, from which silica was solubilized and then reprecipitated on fracture planes, which formed the PrOSV veins. The next two events are more closely related to the tungsten mineralization. Initially, following albitization and microclinization, CO_2-bearing, Na- and Cl-rich aqueous solutions exsolved from the crystallizing granitic magma and accumulated at the cupola zones of the Musa batholith (Fig. 8). Pressure build-up led to hydraulic fracturing of the rocks and circulation of the solutions through the open spaces, where OSV veins were formed at estimated pressures of 2 Kbar (Fig. 8). At the upper levels of the deposit, saline aqueous-carbonic fluids ($H_2O + CH_4 + CO_2$ + salts) seem to have resulted from the mixing of metamorphic and magmatic solutions (Fig. 8).

Subsequently, the OSV veins were intensely fractured (Fig. 8), enabling further percolation of the fluids derived from the greenstone host rocks. The circulation of these fluids on the Pedra Preta deposit may have been synchronous with the wolframite precipitation. FI evidence (microthermometric and crushing tests) supports the hypothesis of tungsten precipitating from an aqueous-carbonic solution with high CH_4/CO_2 ratios. Tungsten deposition should have been accompanied by an increase of f_{O_2} in the fluids, thus favoring the coprecipitation of hematite. Oxygen isotope data indicate temperatures of 320 °C for the tungsten deposition, in agreement with the highest Th_{total} of FIs in wolframite and quartz 2.
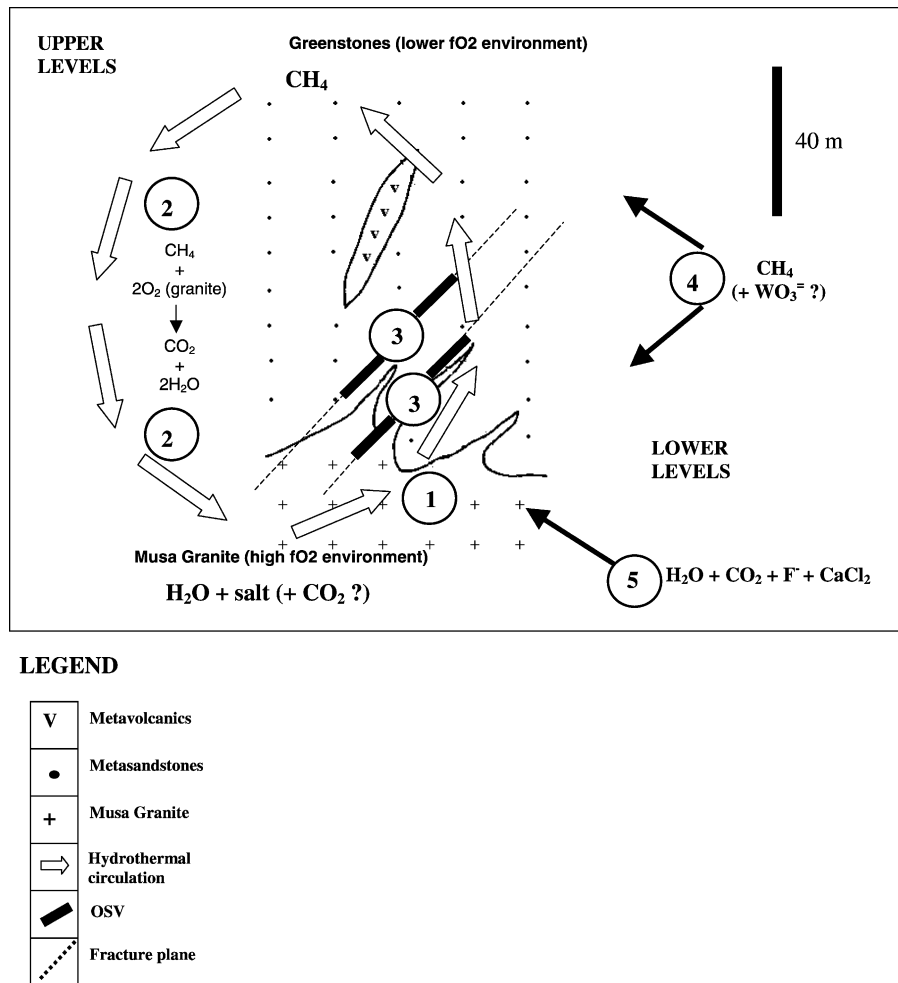
Fig. 8. Proposed evolution model for the Pedra Preta deposit. The last stages of magma crystallization were characterized by albitization, microclinization and accumulation of CO_2-bearing saline aqueous fluids at the upper zones of the granitic body (1), causing fracturing at the cupola. Fluids derived from the host greenstone were reducing (CH_4-rich). In the upper and lower levels of the deposit, during precipitation of quartz 2, there seems to have occurred mixing of magmatic and metamorphic fluids (2). As a consequence of the high f_{O_2} of the granite, CH_4 oxidation produced CO_2. Quartz 2 was precipitated along fractures (3) at pressures of about 2 Kbar, and OSV were then formed. Subsequently, the OSV veins were fractured, allowing further circulation of the reducing fluids derived from the greenstone host rocks (4). The inflow of these fluids may have been coeval with wolframite precipitation. Oxygen isotopic data indicate temperatures around 320 °C for the tungsten deposition. Micro-displacements in quartz 2 modified primary FI and CH_4 changed partially to CO_2. Fluorination (5) was certainly effected by $H_2O + F^- + CO_2 + CaCl_2$ fluids, which may have been related to a concealed specialized plutonic facies of the Musa granite.

The Pedra Preta system then experienced an F-metasomatism (Fig. 8) by fluids that probably were related to later differentiates or to a facies of the Musa granite not yet exposed by erosion. These solutions, enriched in Na^+, K^+, Ca^{++}, Al^{+3}, F^-, and H_4SiO_4, caused greisenization of the granite cupola, where topaz and fluorite were deposited in thermal conditions of $\approx 240-350$ °C. They also ascended along the OSV fractures to the upper levels, where they deposited mainly topaz, fluorite, and sericite. In the metamafic and metasedimentary host rocks, phengite-rich alteration haloes were developed around the veins.

Topaz precipitated from heterogeneous fluids at an average temperature of 320 °C. These fluids had an aqueous-carbonic composition with low CO_2 density and a Ca-rich aqueous phase. By the time fluorite precipitated, X_{CO_2} decreased to < 0.1 in the Na^+- and Ca^{++}-rich aqueous solutions. This stage is also characterized by the partial

substitution of wolframite by scheelite, as a direct consequence of the high a_{Ca++} of the fluids.

The last hydrothermal event is represented by the POSV vein formation. The corresponding aqueous solutions were moderately to highly saline ($\approx 12-42$ wt% $CaCl_2$) and relatively hot (< 220 °C). Fluids with the highest $CaCl_2$ content were trapped in quartz 3 from the granite cupola and could have been exsolved from the granitic residual melts. The low eutectic temperatures of these fluids may be due to Li^+ ions in solution, as often occurs in fluids of pegmatite affiliation, or represent metastable eutectic behavior of the $H_2O-NaCl-CaCl_2$ system. Na-rich brines moved next into the deposit, though in a restricted way. Most likely, the fluids from which both the POSV veins and those at the northern border of the Musa granite were formed have a pegmatitic origin or represent connate or deep groundwater.

From the FI data, a general dilution of the aqueous solutions after the initial percolation of the Na-rich brines can be inferred. Chloritization occurs throughout the deposit and is a common alteration on feldspars and micas. Minor sulfide deposition is largely contemporaneous with chloritization. As the alteration advanced and most of the sulfides were deposited, H^+ bulk concentration progressively decreased to the point that pH conditions favored the precipitation of calcite. The last fluids to circulate as part of the Pedra Preta hydrothermal system were probably responsible for the formation of quartz 4. These fluids are characterized by colder, very dilute solutions and most likely represent shallow groundwater.

The Pedra Preta deposit has several common features with other wolframite deposits associated with granitoids, but it differs from them in some aspects that are generally described in classical metallogenetic models (Kwak et al., 1982; Sobolev, 1991). Although the spatial relationship with the Musa batholith is obvious, its genetic affiliation is less evident because the granitic facies associated with the Pedra Preta deposit is neither specialized (Gastal, 1987) nor characterized as an S-type granitic rock (Gastal, 1987; Dall'Agnol and Magalhães, 1995). In this study, fluid data support the transport of W by solutions with strong nonmagmatic contributions, from which the metallic load was deposited in fractures opened in the host OSV veins. Evidence for this hypothesis comes from the reducing character of the fluids (high CH_4 content) that migrated throughout the deposit after the precipitation of quartz 2 and possibly during the wolframite deposition.

The thermal energy released as a consequence of the Musa granite cooling caused the convective movement of the solutions through the host rocks. Whether the Andorinhas supergroup rocks were a suitable source for W is open to debate, as is the Musa granite itself, considering that a more specialized facies has not yet been mapped. Whether this facies exists is speculation, but it would account for the F-metasomatism observed in the deposit.

A dual origin of the tungsten in the Pedra Preta deposit (magmatic and/or metamorphic) seems atypical. First, in wolframite deposits associated with granitoids, the source of tungsten is usually intrusive rocks. Second, no W deposit associated with Precambrian granitoids has been interpreted as of magmatic affiliation (Sobolev, 1991), though Raith and Prochaska (1995) record a W–Mo deposit spatially and genetically related to a 1.1 Ga granitoid.

Acknowledgements

References

Althoff, F.J., Barbey, P., Boullier, A.M., Dall'Agnol, R., 1995. Composição e estrutura dos granitóides arqueanos da região de Marajoara. Bol. Mus. Para. Emilio Goeldi, Sér. Ciênc. Terra 7, 5–26.

Araujo, O.J.B., Maia, R.G.N., João, X.S.J., Costa, J.B.S., 1988. A megaestruturação arqueana da folha Carajás. Simp. Latino Americano Geol. 7, Belém, SBG, Anais 1, 324–333.

Avelar, V.G., Lafon, J.M., Correia, F.C. Jr., Macambira, E.M.B., 1999. O magmatismo arqueano da região de Tucumã. Provincia Mineral de Carajás: Novos Resultados Geocronológicos.

Baker, T., 1998. Alteration, mineralization and fluid evolution at the Eloise Cu–Au deposit, Cloncurry district, northwest Queensland, Australia. Econ. Geol. 93 (8), 1213–1236.

Blevin, P.L., Chappell, B.W., 1992. The role of magma sources, oxidation states and fractionation in determining the granite metallogeny of eastern Australia. Trans. R. Soc. Edinburgh: Earth Sci. 83, 305–316.

Bernard, A., Symonds, R.B., Rose, W.I., 1990. Volatile transport and deposition of Mo, W and Re in high temperatures magmatic fluids. Fluid Inclusions Res. 23, 15.

Bodnar, R.J., Vityk, M.O., 1994. Interpretation of microthermometric data for H_2O–NaCl fluid inclusions. In: De Vivo, B., Frezzotti, M.L. (Eds.), Fluid Inclusions in Minerals: Methods and Applications: Short Course of the Working Group (IMA), Pontignano, Siena, Italy, pp. 117–130.

Campbell, A.R., Robinson Cook, S., 1987. Infrared fluid inclusion microthermometry on coexisting wolframite and quartz. Econ. Geol. 82, 1640–1645.

Campbell, A.R., Hackbarth, C.J., Plumlee, G.S., Petersen, U., 1984. Internal features of ore minerals seen with the infrared microscope. Econo. Geol. 79, 1387–1392.

Cheilletz, A., 1984. Caractéristiques géochimiques et termobarométriques des fluides associe's à la scheelite et au quartz des mineralisations de tungstène du Jbel Aouam (Maroc Central). Bull. Miner. 107, 255–272.

Cordeiro, A.A.C., da Silva, A.V., 1986. Depósito de wolframita da região da Pedra Preta, Pará. In: Schobbenhaus, C., Coelho, C.E.S. (Eds.), Principais Depósitos Minerais do Brasil, DNPM-CVRD 2, pp. 409–416.

Cordeiro, A.A.C., Alves, C.A.S., Biagini, D.O., Fonseca, L.R., Nascimento, J.A.S., Azevedo, I.L., Santos, F.F., 1988. Depósito de wolframita de Pedra Preta, sul do Pará. Cong. Bras. Geol., Anexo aos anais (Província Mineral de Carajás), Belém, SBG 35, 159–165.

Dall'Agnol, R., Magalhães, M.S., 1995. Geochemistry and petrogenesis of the anorogenic Jamon and Musa granites, Eastern Amazonian Craton, Brazil: implications for the genesis of A-type proterozoic granites. Int. Symp. Rapakivy Granites and related rocks. Extended Abstracts, Belém, 22–23.

Dall'Agnol, R., Lafon, J.M., Macambira, M.J.B., 1994. Proterozoic anorogenic magmatism in the Central Amazonian province, Amazonian Craton: geochronological, petrological and geochemical aspects. Mineral. Petrol. 50, 113–138.

Dall'Agnol, R., Rämo, O.T., Magalhães, M.S., Macambira, M.J.B., 1999a. Petrology of the anorogenic, oxidised Jamon and Musa granites, Amazonian Craton: implications for the genesis of the Proterozoic A-type granites. Lithos 46, 431–462.

Dall'Agnol, R., Scaillet, B., Pichavant, M., 1999b. An experimental study of a Lower Proterozoic A-type granite from the Eastern Amazonian Craton, Brazil. J. Petrol. 40, 1673–1698.

Davis, D.W., Olwenstein, T.K., Spencer, R., 1990. Melting behavior of fluid inclusions in laboratory-grown halite crystals in the systems NaCl–H_2O, NaCl–KCl–H_2O, NaCl–$MgCl_2$–H_2O and NaCl–$CaCl_2$–H_2O. Geochim. Cosmochim. Acta 54, 591–601.

Dias, G.S., Macambira, M.J.B., Dall'Agnol, R., Soares, A.D.V., Barros, C.E.M., 1996. Datação de zircão de silll de metagabro: comprovação da idade arqueana da Formação Águas Claras, Pará. Simp. Geol. Amaz. 5, Belém, SBG, Bol. Resumos Expandidos, 376–379.

Docegeo, 1984. Relatorio Final de Pesquisa: Area Pedra Preta, Docegeo-CVRD, vol. 1., 110p.

Durisova, J., Sztacho, P., Dubessy, J., 1992. A fluid inclusion study of Au–W stratiform mineralization at Orlík near Humpolec, Czechoslovakia. Eur. J. Miner. 4, 965–976.

Fernandez, R.R., 1991. Mineral deposition in the La Bismutina ore deposit, Argentina. In: Pagel, M., Leroy, J.L. (Eds.), Source, Transport and Deposition of Metals, Balkema, Rotterdam, pp. 33–36.

Frape, S.K., Fritz, P., 1987. Geochemical trends for groundwaters from the Canadian Shield. Geol. Assoc. Can. Spec. Pap., 19–39.

Fuzikawa, K., 1982. Fluid inclusions and oxygen isotope studies of the Nabarlek uranium deposit NT Australia. Unpublished PhD thesis, University of Adelaide, 226pp.

Fuzikawa, K., 1985. Inclusões fluidas: métodos usuais de estudo e aplicações. Contribuições a Geologia e Petrologia. SBG-Núcleo Minas Gerais, 29–44.

Gastal, M.C., 1987. Maçico granítico Musa: mapeamento, petrologia e petroquímica. Unpublished MSc thesis, Federal University of Pará, Brazil, 307pp.

Gerstner, M.R., Bowman, J.R., Pasteris, J.D., 1989. Skarn formation at the MacMillan Pass tungsten deposit (MacTung), Yukon and Northwest territories. I. P–T–X–V characterization of the metane-bearing skarn forming fluids. Can. Miner. 27, 545–563.

Giuliani, G., 1984. Les concentrations filoniennes à tungstène-étain du massif granitique des Zaër (Maroc Central): minéralisations et phases fluides associées. Miner. Deposita 19, 193–201.

Guha, J., Kanwar, R., 1987. Vug brines-fluid inclusions: a key to the understanding of secondary gold enrichment processes and the evolution of deep brines in the Canadian Shield. Geol. Assoc. Can. Spec. Pap. 33, 96–101.

Gumiel, J.C., Quilez, E., Vindel, E., Beny, C., 1989. Fluid inclusion study of San Nicolas W–Sn–Bi–Mo greisen deposit, Extremadura, Western Spain. ECROFI 10, 42Abstracts, London.

Higgins, N.C., 1980. Fluid inclusion evidence for the transport of tungsten by carbonate complexes in hydrothermal solutions. Can. J. Earth Sci. 17, 823–830.

Higgins, N.C., 1985a. Wolframite deposition in a hydrothermal vein system: the Grey River tungsten prospect, Newfoundland, Canada. Econ. Geol. 80, 1297–1327.

Higgins, N.C., 1985b. Moderately depleted oxygen isotope compositions of waters associated with tin- and tungsten-bearing quartz veins: an evaluation of isotopic models. In: Herbert, H.K., So, S.E. (Eds.), Stable Isotopes and Fluid Pressures in Mineralization, Publication 23, University of Western Australia, pp. 204–214.

Hirata, W.K., Rigon, J.C., Kadekaru, K., Cordeiro, A.A.C., Meireles, E., 1982. Geologia regional da Província Mineral de Carajás. Simp. Geol. Amaz. 1, Proceedings, Belém, 100–110.

Ishihara, S., 1981. The granitoid series and mineralization. Econ. Geol., Anniv. Vol. 75, 458–484.

Jaireth, S., Heinrich, C.A., Solomon, M., 1990. Chemical controls on hydrothermal tungsten transport and the precipitation of ferberite and wolframite. Geol. Soc. Aust. Abstr. 25, 269–270.

Kilias, S.P., Konnerup-Madsen, J., 1997. Fluid inclusion and stable isotope evidence for the genesis of quartz-scheelite veins, Metaggitsi area, central Chalkidiki peninsula, N. Greece. Miner. Depósita 32, 581–595.

Krauskopf, K.B., 1967. Introduction to Geochemistry, Mc Graw-Hill, New York, 721pp.

Krauskopf, K.B., 1974. Tungsten. In: Wedepohl, K.H., (Ed.), Handbook of Geochemistry, Springer, Berlin, pp. 74B-1–74O-1.

Kwak, T.A.P., Taylor, R.G., Plimer, I.R., 1982. Australian tungsten deposits. In: Hopworth, J.V., Zhang, Y.H. (Eds.), Tungsten Geology Symposium, Jiangxi, China, pp. 127–152.

Luders, V., Ziemann, M., 1999. Possibilities and limits of infrared light microthermometry applied to studies of pyrite-hosted fluid inclusions. Chem. Geol. 154 (1–4), 169–178.

Macambira, M.J.B., Lafon, J.M., 1994. Geocronologia da Província Mineral de Carajás: síntese dos resultados e novos desafios. Simp. Geol. Amaz. 4, SBG, Belém, Bol. Resumos Expandidos, 339–342.

Macambira, M.J.B., Lancelot, J., 1991. Em busca do embasamento arqueano de Rio Maria, SE do Estado do Pará. Simp. Geol. Amaz. 3, SBG, Belém, Anais, 49–58.

Macambira, M.J.B., Lancelot, J., 1992. Idade U–Pb em zircões de metavulcânicas do 'greenstone' do Supergrupo Andorinhas, delimitante da estratigrafia arqueana de Carajás, Estado do Pará. Cong. Bras. Geol. 37, SBG, São Paulo, Anais 2, 188.

Machado, N., Lindenmeyer, Z., Kroch, T.E., Lindenmeyer, D., 1991. U–Pb geochronology of Archean magmatism and basement reactivation in Carajás Area, Amazon Shield, Brazil. Precambrian Res. 49 (3–4), 329–354.

Magalhães, M.S., Dall'Agnol, R., 1992. Estudos de minerais opacos e suscetibilidade magnética nos granitos Musa e Jamon (Região de Rio Maria-SE do Pará) e suas implicações petrológicas. Rev. Bras. Geoc. 22, 184–197.

Mancano, D.P., Campbell, A.R., 1995. Microthermometry of enargite hosted fluid inclusions from Lepanto, Phillipines, high sulfidation Cu–Au deposit. Geochim. Cosmochim. Acta 59 (19), 3909–3916.

Marignac, C., Cuney, M., 1991. What is the meaning of granite specialization for Sn, W deposit genesis? . In: Pagel, M., Leroy, J.L. (Eds.), Source, Transport and Deposition of Metals, Balkema, Brookfield, pp. 771–774.

Moura, C.A.V., Gaudette, H.E., 1993. Evidência de deformação brasiliana/panafricana no Cinturão Araguaia: implicações para a evolução do Gondwana. Rev. Bras. Geoc. 23, 117–123.

Naumov, V.B., Ivanova, G.F., 1971. The pressure and temperature conditions for formation of wolframite deposits. Geochem. Int. 8, 381–394.

Noronha, F., Doria, A., Dubessy, J., Charoy, B., 1992. Characterization and timing of the different types of fluids present in the barren and ore veins of the W–Sn deposit of Panasqueira, Central Portugal. Miner. Deposita 27, 72–79.

O'Reily, C., Gallagher, V., Feely, M., 1997. Fluid inclusion study of the Ballinglen W–Sn sulphide mineralization, SE Ireland. Miner. Deposita 32, 569–580.

Quilez, E., Sierra, J., Vindel, E., 1989. A fluid inclusion study and genetic model of wolframite quartz veins, Garganta de los Montes, Spanish Central System. Fluid Inclusions Res. 22, 301–302.

Pimentel, M.M., Machado, N., 1994. Geocronologia U–Pb dos terrenos granito-greenstones de Rio Maria, Pará. Cong. Bras. Geol. 38, SBG, Camboriu, Bol. Resumos Expandidos 2, 390–391.

Polya, D.A., 1989. Chemistry of the main stage ore forming fluids of the Panasqueira W–Cu(Ag)–Sn deposit, Portugal: Implications for models of ore genesis. Econ. Geol. 84, 1134–1152.

Ramboz, C., Schnapper, D., Dubessy, J., 1985. The P–V–T–X–f_{O_2} evolution of H_2O–CO_2–CH_4 bearing fluid in a wolframite vein: reconstruction from fluid inclusion studies. Geochim. Cosmochim. Acta 49, 205–219.

Raith, J.G., Prochaska, W., 1995. Tungsten deposits in the Wolfram Schist, Namaqualand, South Africa: strata-bound versus granite related genetic concepts. Econ. Geol. 90, 1934–1954.

Richards, J.P., Kerrich, R., 1993. Observations of zoning and fluid inclusions in pyrite using a transmitted infrared light microscope. Econ. Geol. 88, 716–723.

Rios, F.J., 1995. A jazida de wolframita de Pedra Preta, Granito Musa, Amazônia Oriental (PA): estudos dos fluidos mineralizantes e isótopos estáveis de oxigênio em veios hidrotermais. Unpublished PhD thesis, Federal University of Pará, 215pp.

Rios, F.J., Villas, R.N., Fuzikawa, K., Sial, A.N., Mariano, G., 1998. Isótopos de oxigênio e temperatura de formação dos veios mineralizados com wolframita da Jazida Pedra Preta, sul do Pará. Rev. Bras. Geoc. 28, 253–256.

Rodrigues, E., Lafon, J.M., Scheller, T., 1992. Geocronologia Pb–Pb da Província Mineral de Carajás: primeiros resultados. Simp. Cong. Bras. Geol. 37, SBG, São Paulo, Bol. Resumos Expandidos 2, 183–184.

Roedder, E., 1984. Fluid inclusions. Rev. Mineral., Mineral. Soc. Am. 12, 644.

Santos, J.F.D., 1987. Tipologia e gênese do depósito de tungstênio de Pedra Preta (PA). Unpublished MSc. thesis, University of São Paulo, Brazil, 93pp.

Schwartz, M.O., Surjono, S., 1990. Greisenization and albitization at the Tikus tin–tungsten deposit, Belitung, Indonesia. Econ. Geol. 85, 691–713.

Seitz, J.C., Pasteris, J.D., 1990. Theoretical and practical aspects of differential partitioning of gases by clathrate hydrates in fluid inclusions. Geochim. Cosmochim. Acta 54, 631–639.

Shieh, Y., Zhang, G.X., 1991. Stable isotopes studies of quartz-vein type tungsten deposits in Dajishan Mine, Jiangxi Province, Southeast China. Geochem. Soc., Spec. Publ., 425–435.

Sial, A.N., Mariano, G., Ferreira, V.P., 1992. Análises de isótopos de oxigênio em silicatos, e oxigênio e carbono em carbonatos: o laboratório de isótopos estáveis da UFPE. Cong. Bras. Geol. 37, SBG, São Paulo, Anais 2, 66–67.

Sillitoe, R.H., 1996. Granites and metal deposits. Episodes 19, 126–133.

Slov'ev, S.G., 1990. Evolution of the composition and state of the post-magmatic fluid of the Kensu cooper–molybdenum–tungsten deposit (Eastern Kirgiziya). Fluid Inclusions Res. 23, 200–202.

So, C.S., Yun, S.T., 1994. Origin and evolution of W–Mo-producing fluids in a granitic hydrothermal system: geochemical studies of quartz vein deposit around Susan granite, Hwanggangri district, Republic of Korea. Econ. Geol. 89, 246–267.

Sobolev, R.N., 1991. Tungsten-bearing granites. In: Pagel, M., Leroy, J.L. (Eds.), Source, Transport and Deposition of Metals, Balkema, Rotterdam, pp. 815–816.

Taylor, H.P. Jr., Epstein, S., 1962. Relationships between $^{18}O/^{16}O$ ratios in coexisting minerals of igneous and metamorphic rocks. Geol. Soc. Am. Bull. 73, 461–480.

Walker, R.T., Samson, I.M., 1998. Cryogenic Raman spectroscopic investigations of fluid inclusions in the NaCl–CaCl$_2$–H$_2$O system. In: Schandl, E., (Ed.), 17th General Meeting, International Mineralogical Association, Toronto, p. A33.

Willing, C.D., 1986. Geologia do tungstênio. In: Schobbenhaus, C., Coelho, C.E.S. (Eds.), Principais depósitos minerais do Brasil, DNPM-CVRD 2, pp. 387–391.

Wood, A.S., Samson, I.M., 2000. The hydrothermal geochemistry of tungsten in granitoid environments: I. Relative solubilities of ferberite and scheelite as a function of T, P, pH and m_{NaCl}. Econ. Geol. 95, 143–182.

Wood, S.A., Vlassopoulos, D., 1989. Experimental determinations of the hydrothermal solubility and speciation of tungsten at 500 °C and 1 Kb. Geochim. Cosmochim. Acta 53, 303.